

AMP-Net: Denoising based Deep Unfolding for Compressive Image Sensing

Zhonghao Zhang *Student Member, IEEE*, Yipeng Liu *Senior Member, IEEE*, Jiani Liu, Fei Wen, Ce Zhu
Fellow, IEEE

Abstract

Most compressive sensing (CS) reconstruction methods can be divided into two categories, i.e. model based methods and classical deep network methods. By unfolding the iterative optimization algorithm for model based methods into networks, deep unfolding method has the good interpretation of model based methods and the high speed of classical deep network methods. In this paper, to solve the visual image CS problem, we propose a deep unfolding model dubbed AMP-Net. Rather than learning regularization terms, it is established by unfolding the iterative denoising process of the well-known approximate message passing algorithm. Furthermore, AMP-Net integrates deblocking modules in order to eliminate the blocking artifact that usually appears in CS of visual image. In addition, the sampling matrix is jointly trained with other network parameters to enhance the reconstruction performance. Experimental results show that the proposed AMP-Net has better reconstruction accuracy than other state-of-the-art methods with high reconstruction speed and a small number of network parameters.

Index Terms

compressed sensing, deep unfolding, approximate message passing, image denoising, image reconstruction.

I. INTRODUCTION

Compressive sensing (CS) requires much fewer measurements than the classical Nyquist sampling to reconstruct a signal [1]. It has been applied in a series of imaging applications, including single-pixel camera [2], magnetic resonance imaging (MRI) [3], and snapshot compressive imaging (SCI) [4].

CS performs fast imaging by sampling only few measurements, i. e. $\mathbf{y} = \mathbf{Ax}$, where $\mathbf{x} \in \mathbb{R}^N$ is the original signal, $\mathbf{y} \in \mathbb{R}^M$ consists of the samples, $\mathbf{A} \in \mathbb{R}^{M \times N}$ is the sampling matrix with $M < N$. The image recovery from compressive samples is to solve an under-determined linear inverse system, and the corresponding optimization model can be formulated as follows:

$$\min_{\mathbf{x}} \Re(\mathbf{x}), \text{ s. t. } \mathbf{y} = \mathbf{Ax}, \quad (1)$$

where $\Re(\mathbf{x})$ is the regularization term.

To solve this optimization problem, model based recovery methods exploit some data structures by employing structure-inducing regularizers [5], such as sparsity in some transformation domains [6], [7], [8], low rank [9], [10], [11], [12], and so on [13], [14], [15], [16], [17]. A number of non-linear iterative algorithms can be used to solve these optimization problems [18], [19], [10], such as sparse Bayesian learning [20], orthogonal matching pursuit (OMP) [21], fast iterative shrinkage-thresholding algorithm (FISTA) [22], approximate message passing (AMP) [23], etc. These methods usually have theoretical guarantees.

In these years, some deep learning based methods have been developed for the image recovery problem [24]. Classical deep networks based methods directly map the compressive samples as input to the estimation as output [25], [26], [27], [28], [29]. These networks consist of stacked non-linear operational layers, such as autoencoders, convolutional neural network (CNN) [30], generative adversarial networks (GANs) [31], etc. Their parameters can be trained by the well-known back propagation algorithm. Compared with the iterative optimization algorithms, these classical deep neural networks can quickly reconstruct images. Nevertheless, due to the black box characteristic of these classical networks, there is no good interpretation and theoretical guarantee. This completely data-driven

This research is supported by National Natural Science Foundation of China (NSFC, No. 61602091, No. 61571102) and the Sichuan Science and Technology program (No. 2019YFH0008, No. 2018Y0035). The corresponding author is Yipeng Liu.

Zhonghao Zhang, Yipeng Liu, Jiani Liu and Ce Zhu are with School of Information and Communication Engineering, University of Electronic Science and Technology of China (UESTC), Chengdu, 611731, China. (email:yipengliu@uestc.edu.cn).

Fei Wen is with the Department of Electronic Engineering, Shanghai Jiao Tong University, Shanghai 200240, China.

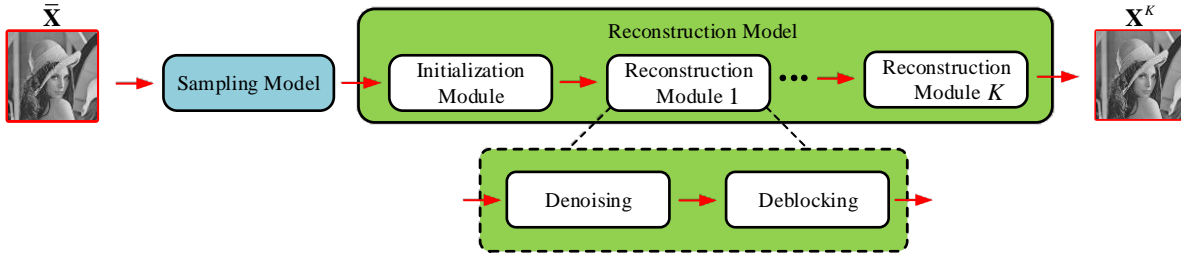


Fig. 1. The framework of AMP-Net. $\bar{\mathbf{X}}$ denotes the original image and \mathbf{X}^K denotes the reconstructed image.

end-to-end manners may have risk for some undesired effects [32]. Therefore, it can be beneficial to integrate prior knowledge and the structure of the operators.

Motivated by the iterative algorithm that processes data step by step, deep unfolding maps iterative restoration algorithms onto deep neural networks [33], [34], [35], [36]. It tries to make compromise between the iterative recovery methods and network methods, and enjoys a good balance between reconstruction speed and interpretation. Deep unfolding methods were first developed to solve the sparse linear inverse problem and the unfolded algorithms include ISTA [33], [37], AMP [38] and iterative hard thresholding (IHT) algorithm [39]. However, it is usually necessary for these methods to obtain additional pre-trained dictionaries to recover images.

In recent years, some non-linear iterative algorithms are unfolded to solve image CS problems. For example, ADMM are unfolded to reconstruct MRI [35] and SCI [4], and primal-dual algorithm is developed to reconstruct CT [40]. ISTA [34], the half-quadratic splitting (HQS) algorithm [36] and linear inverse operation [41] are exploited to solve the CS of visual image problem. Some methods [35], [4], [34] design deep unfolding models by pre-assuming specific regularizers, such as ℓ_1 norm for sparsity in some basis. Carefully designed regularization terms are intuitive, but may ignore other image intrinsic structures. It has been proved that combining multiple kinds of image prior knowledges can get better reconstruction results than single one [11], [12], [42]. To integrate more information, some methods use deep networks to model an appropriate regularizer [34], [40], [36], [41]. But due to the uncertainty and unrepresentability of the regularizer, it is difficult to learn the the regularizer directly. Instead, some information related to the regularizer are learned, such as denoising prior [36], gradient [43], inverse information [41]. However, to learn these information, classical deep neural networks usually contain a large amount of parameters, which makes the application of related models limited. In this paper, we establish the deep unfolding model by unfolding the iterative denoising process from the denoising perspective of the AMP algorithm.

The AMP algorithm interprets a classical linear operation $\mathbf{A}^T(\mathbf{A}\mathbf{x}' - \mathbf{y}) + \mathbf{x}'$ as the sum of the original data and a noise term [23], where $\mathbf{x}' \in \mathbb{R}^N$ is the data with different values from \mathbf{x} . To obtain the original data, related non-linear operations in each iteration can be regarded as a series of denoising processes which depend on different image priors. In this paper, we call this interpretation as the denoising perspective of the AMP algorithm. This perspective provides a more flexible way to better fit the characteristics of images. Rather than learning regularizer-based information, from this perspective, image prior can be presented by learning denoising operators or directly fitting the noise term in each iteration. Such a strategy makes the representation of the image prior more flexible and intuitive with fewer demanded parameters.

Besides, in CS systems, visual images are commonly sampled block by block and reconstructed by processing each image block [44], [26], [27], [34]. However, for these block-based methods, additional deblocking operations must be applied to eliminate blocking artifact, resulting in a significant amount of time consumption [27]. Some classical deep networks perform reconstructing image reconstruction and deblocking at the same time [28], [29]. Similarly, we integrate deblocking operations into the reconstruction process of the proposed deep unfolding model.

In addition, recent sampling matrix training strategy is employed in some model based methods and classical deep neural networks [17], [28]. In such a strategy, the sampling matrix is trained with other parameters using gradient descend related algorithms [45]. Since the sampling matrix plays an important role in both sampling and reconstruction in most deep unfolding methods [34], [36], [41], an appropriate sampling matrix may effectively improve the reconstruction performance. In this work, the sampling matrix is jointly trained with other parameters of the designed deep unfolding model.

In this paper, we propose a novel deep unfolding model dubbed AMP-Net to solve the visual image CS problem.

Fig. 1 illustrates the framework of AMP-Net. AMP-Net is composed of a sampling model and a reconstruction model. In sampling model, images are measured block-by-block using the same sampling matrix. The reconstruction model is established by unfolding the iterative denoising process, which is inspired from the denoising perspective of the AMP algorithm. The reconstruction model is an unfolding form of the denoising process with K iterations. It consists of an initialization module and K reconstruction modules. The initialization module is used to generate a reasonable initial estimation. Each reconstruction module containing a denoising module and a deblocking module. The denoising module processes each image block, and deblocking module is for the whole image. Experimental results demonstrate that the proposed method outperforms the state-of-the-art ones in terms of reconstruction accuracy and computational complexity.

The main contributions of this paper can be summarized as follows:

- We develop a novel deep unfolding model named AMP-Net which is inspired by the denoising perspective of the AMP algorithm. Different from other methods, the reconstruction model is established by unfolding the iterative denoising process, rather than modelling the regularizers using various non-linear iterative algorithms.
- To eliminate the blocking artifact, a deblocking module is designed following the denoising module. To the best of our knowledge, this is the first work which integrates deblocking operations into a deep unfolding model.
- We jointly train the sampling matrix with other parameters of AMP-Net due to its contributions in both sampling and reconstruction. In this way, AMP-Net can obtain an data-driven sampling matrix for visual images.

The paper is organized as follows. Section II introduces some related works and the denoising perspective of the AMP algorithm. Section III describes AMP-Net in detail. Section IV is the experimental results. And in Section V, we conclude this paper and discuss the future works.

II. BACKGROUND

In this section, some works related to AMP-Net are presented and the denoising perspective of the AMP algorithm is introduced.

A. Related Works

Model based methods are based on regularization terms inspired by image priors. Sparsity in some transformation domains, such as DCT [6], wavelet [46] and gradient domain [44], was exploited to reconstruct visual images. For example, Li et al. [44] used a second order total variation (TV) regularizer to build an optimization problem and applied the augmented Lagrangian method to recover each image block. However, fixed domain may result in poor performance. To improve the reconstruction performance, some elaborate priors are exploited, such as denoising prior [14], [15] and network prior [16], [17]. Specifically, in [14], BM3D denoiser was combined with the AMP algorithm to develop a new framework named D-AMP for image reconstruction. In [17], Wu et al. employed a pre-trained deep neural network to represent the image prior and applied three times of gradient descend to reconstruct images. In this framework namely DCS, the sampling matrix is pre-trained.

For classical deep network methods, Mousavi et al. [26] designed a stacked denoising autoencoder (SDA) to reconstruct images from sampled data for the first time. After that, Kulkarni et al. [27] proposed a CNN based model namely ReconNet to improve the reconstruction of visual images. And a sampling-reconstruction framework called CSNet is proposed to erase the blocking artifact and further enhance the performance [28]. Meanwhile, the sampling matrix and the reconstruction model are jointly trained.

Deep unfolding methods combine the advantages of model based methods and classical deep network methods. For visual image reconstruction, recently, a deep unfolding model named ISTA-Net [34] was proposed to solve an optimization problem with a sparsity-inducing regularizer using nonlinear transforms. ISTA-Net employed CNNs to the transformation operations and trainable soft thresholding functions to reflect the sparsity of data. Dong et al. [36] designed a deep unfolding model dubbed DPDNN to solve common inverse problems by unfolding the denoising process inspired by HQS method. Although DPDNN uses the denoising prior, but it has a different structure from AMP-Net. Gilton et al. [41] developed a deep unfolding model named Neumann Network (NN) for common image inverse problems by truncating Neumann series with a data-driven non-linear regularizer. These methods pay much attention to analyzing and modelling regularization terms.

In fact, derived by the denoising perspective of AMP algorithm, the proposed AMP-Net has distinct features compared with all these existing methods for visual image CS problem. Specially, unlike model based methods, AMP-Net unfold the iterative reconstruction to a fixed trainable forward propagation process, which uses less time for reconstruction. Different from classical deep network methods, AMP-Net uses the sampling matrix in the reconstruction process to improve the performance, and the sampling matrix is trained with other parameters. Furthermore, AMP-Net is established by unfolding the iterative denoising process and fitting the noise term from the denoising perspective of the AMP algorithm rather than modelling the regularization term.

B. The Denoising Perspective of the AMP Algorithm

In this subsection, we will introduce the denoising perspective of the AMP algorithm. The AMP algorithm analyzes a classical scheme of iterative non-linear algorithms [22], [23] as follows:

$$\mathbf{z}^{k-1} = \mathbf{y} - \mathbf{A}\mathbf{x}^{k-1}, \quad (2)$$

$$\mathbf{x}^k = \mathfrak{T}_k(\mathbf{A}^T \mathbf{z}^{k-1} + \mathbf{x}^{k-1}), \quad (3)$$

where \mathbf{A}^T is the transpose of sampling matrix \mathbf{A} , $\mathfrak{T}_k(\cdot)$ is the non-linear function, and k is the number of iterations. If the initialized input and the original data are defined as \mathbf{x}^0 and $\bar{\mathbf{x}}$, then we can have

$$\mathbf{A}^T \mathbf{z}^0 + \mathbf{x}^0 = \bar{\mathbf{x}} + (\mathbf{A}^T \mathbf{A} - \mathbf{I})(\bar{\mathbf{x}} - \mathbf{x}^0), \quad (4)$$

where \mathbf{I} is the identity matrix in the size of $N \times N$. The detailed derivation of (4) can be found in Appendix A. By extending (4) to the k -th iteration, we can get

$$\mathbf{A}^T \mathbf{z}^{k-1} + \mathbf{x}^{k-1} = \bar{\mathbf{x}} + (\mathbf{A}^T \mathbf{A} - \mathbf{I})(\bar{\mathbf{x}} - \mathbf{x}^{k-1}), \quad (5)$$

where the entries \mathbf{A}_{ij} of the sampling matrix are independent and identically distributed as $\mathbf{A}_{ij} \sim \mathcal{N}(0, 1/M)$, and $\mathcal{N}(\mu, \sigma^2)$ denotes the Gaussian distribution with the mean value μ and the variance σ^2 . Under this assumption, it can be proved that $(\mathbf{A}^T \mathbf{A} - \mathbf{I})(\bar{\mathbf{x}} - \mathbf{x}^{k-1})$ is also a Gaussian distributed vector with the variance $M^{-1} \|\bar{\mathbf{x}} - \mathbf{x}^{k-1}\|_2^2$ [23]. Then, (5) can be reformulated into the sum of the original signal and a noise term as follows:

$$\mathbf{A}^T \mathbf{z}^{k-1} + \mathbf{x}^{k-1} = \bar{\mathbf{x}} + \mathbf{e}, \quad (6)$$

where $\mathbf{e} = (\mathbf{A}^T \mathbf{A} - \mathbf{I})(\bar{\mathbf{x}} - \mathbf{x}^{k-1})$ denotes the noise term.

The AMP algorithm interprets the non-linear function $\mathfrak{T}_k(\cdot)$ as a denoising function varying with different signal priors. For example, if signals are assumed to be sparse without value limitation, $\mathfrak{T}_k(\cdot)$ can be the soft thresholding function [22]. In this paper, we call such interpretation as the denoising perspective of the AMP algorithm. And it can be noticed that if $\|\bar{\mathbf{x}} - \mathbf{x}^{k-1}\|_2^2$ decreases in each iteration, the Euclidean distance between the reconstruction result and $\bar{\mathbf{x}}$ would get smaller as the iteration number increases.

Significantly, it is worth noting that \mathbf{e} has no relation with the regularizer in model based methods. It is only affected by the original image and the input of each iteration. Therefore, it can be fitted by supervised learning, while the image prior can be learned during the noise term fitting process. Such a strategy makes the representation of the image prior more flexible and intuitive with no need to figure out the specific form of the regularization term. In this study, we employ a classical deep network to fit the noise term end-to-end in each iteration.

III. AMP-NET

In this section, we will illustrate the detail of AMP-Net. As shown in Fig. 1, AMP-Net is composed of a sampling model and a reconstruction model which contains an initialization module and a series of stacked reconstruction modules.

Note that we mainly focus on single-channel images in this study while colourful images can be sampled and recovered channel by channel.

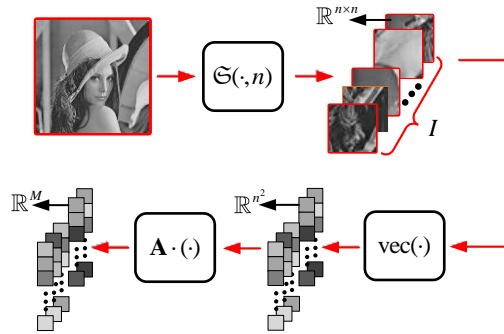


Fig. 2. The sampling process of the sampling model.

A. Sampling Model

The sampling model samples images block by block and is similar to the one in CSNet [28]. However, it is not composed of convolutional kernels but a simple sampling matrix due to its relevance to the reconstruction process.

To demonstrate the sampling process, we denote $\mathfrak{S}(\mathbf{X}, n)$ as a splitting function which divides a single-channel image as $\mathbf{X} \in \mathbb{R}^{L \times P}$ into a series of unoverlaped image blocks. Each image block is denoted as $\mathbf{X}_i \in \mathbb{R}^{n \times n}$, where $i \in \{1, 2, \dots, I\}$ and $L \cdot P = I \cdot n^2$. And $\text{vec}(\cdot)$ is defined as a vectorization function which vectorize an image block to a vector, which satisfies $\text{vec}(\mathbf{X}_i) \in \mathbb{R}^{n^2}$ and $\text{vec}(\mathfrak{S}(\mathbf{X}, n)) \in \mathbb{R}^{n^2 \times I}$. The sampling process of the sampling model is shown in Fig. 2 and can be expressed as

$$\mathbf{Y} = \mathbf{A} \text{vec}(\mathfrak{S}(\mathbf{X}, n)), \quad (7)$$

where $\mathbf{A} \in \mathbb{R}^{M \times n^2}$ is the sampling matrix for image blocks and $\mathbf{Y} \in \mathbb{R}^{M \times I}$ is the measurement. Each column of \mathbf{Y} is the vectorized measurement of an image block.

Moreover, in order to enhance the reconstruction performance of AMP-Net, \mathbf{A} is simultaneously trained with other parameters for its contributions in both sampling and reconstruction. And the derivation of its gradient for updating can refer to Appendix B.

B. Reconstruction Model

Due to the inspiration of the denoising perspective of the AMP algorithm, the reconstruction model is established by unfolding the iterative denoising process. This model is composed of an initialization module and a series of reconstruction modules. The initialization module is used to generate a reasonable initial estimation. The subsequent reconstruction modules are derived by mapping the iterative denoising process onto a deep network. Each module stands for an iteration. And each reconstruction module contains a denoising module and a deblocking module.

Initialization module. The image is initialized by linear operations of the observations. Fig. 3 shows the initialization process. $\mathfrak{S}^{-1}(\cdot, n)$ is defined as a concatenation function which merges all the image blocks into a whole image and satisfies $\mathbf{X} = \mathfrak{S}^{-1}(\mathfrak{S}(\mathbf{X}, n), n)$. Meanwhile, $\text{vec}^{-1}(\cdot)$ is a reshaping function which reshapes the vectorized image to its original shape and satisfies $\mathbf{X}_i = \text{vec}^{-1}(\text{vec}(\mathbf{X}_i))$. The initialization process can be formulated as

$$\mathbf{X}^0 = \mathfrak{S}^{-1}(\text{vec}^{-1}(\mathbf{B}\mathbf{Y})), \quad (8)$$

where $\mathbf{B} \in \mathbb{R}^{n^2 \times M}$ is a trainable matrix for initialization and $\mathbf{X}^0 \in \mathbb{R}^{L \times P}$ denotes the initialized image.

Denoising module. The denoising module is designed to reconstruct each image block. By assuming that $\mathbf{x}_i = \text{vec}(\mathbf{X}_i)$ and inspired by (5), the original data can be obtained by calculating

$$\bar{\mathbf{x}}_i = \mathbf{A}^T \mathbf{z}_i^{k-1} + \mathbf{x}_i^{k-1} - (\mathbf{A}^T \mathbf{A} - \mathbf{I})(\bar{\mathbf{x}}_i - \mathbf{x}_i^{k-1}). \quad (9)$$

If $\bar{\mathbf{x}}_i - \mathbf{x}_i^{k-1}$ is obtained, the reconstruction can be achieved by linear operations. To this end, we replace $\bar{\mathbf{x}}_i - \mathbf{x}_i^{k-1}$ with a non-linear trainable function $\mathfrak{N}_k(\cdot)$ and extend (9) to an iterative version, which can be expressed as

$$\mathbf{x}_i^k = \mathbf{A}^T \mathbf{z}_i^{k-1} + \mathbf{x}_i^{k-1} - (\mathbf{A}^T \mathbf{A} - \mathbf{I}) \text{vec}(\mathfrak{N}_k(\mathbf{X}_i^{k-1})). \quad (10)$$

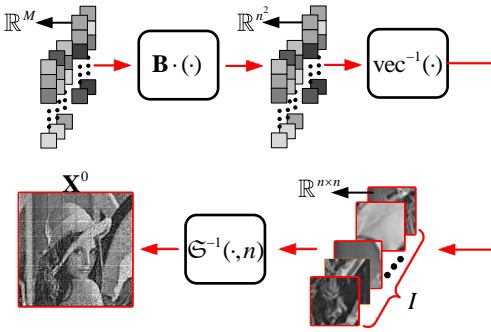
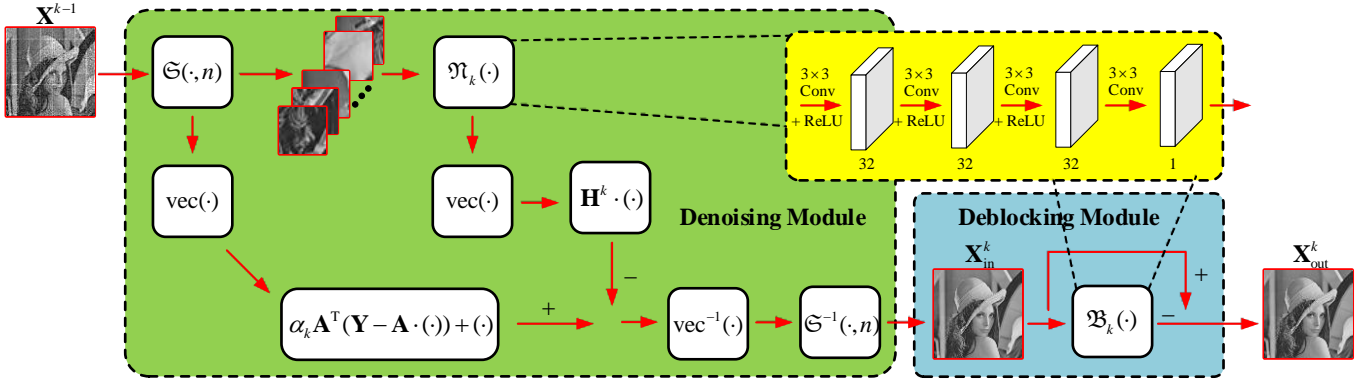


Fig. 3. The initialization process of the initialization module.

Fig. 4. The k -th reconstruction module of AMP-Net.

By regarding $(\mathbf{A}^T \mathbf{A} - \mathbf{I}) \text{vec}(\mathfrak{N}_k(\mathbf{X}_i^{k-1}))$ as the noise term, the reconstruction process in (10) can be interpreted as the denoising process. As we can see, \mathbf{A} play an important role in the reconstruction process (10). If there is an appropriate sampling matrix, the reconstruction performance would get improved. This probably partly explains why the sampling matrix training strategy is effective for recovery.

It is obvious that (11) tries to use $\mathfrak{N}_k(\mathbf{X}_i^{k-1})$ to fit $\bar{\mathbf{X}}_i - \mathbf{X}_i^{k-1}$. In this paper, $\mathfrak{N}_k(\cdot)$ is designed to be a CNN. As shown in Fig. 4, $\mathfrak{N}_k(\cdot)$ is constructed of four convolutional layers, of which the first three layers with bias terms are followed by a Rectified Linear Unit (ReLU) [47] and the last convolutional layer has no bias term. The filter size of each convolutional layer is 3×3 . To make sure that the output has the same size as the input, the padding size of each convolutional layer is set to be 1. The number of output channels for the four convolutional layers are 32, 32, 32, 1, respectively.

Moreover, a trainable parameter α_k is introduced to enhance the flexibility of reconstruction process. With α_k , the iterative reconstruction process can be expressed as

$$\mathbf{x}_i^k = \alpha_k \mathbf{A}^T \mathbf{z}_i^{k-1} + \mathbf{x}_i^{k-1} - (\alpha_k \mathbf{A}^T \mathbf{A} - \mathbf{I}) \text{vec}(\mathfrak{N}_k(\mathbf{X}_i^{k-1})). \quad (11)$$

The detailed derivation of (11) is similar to (10), and can be found in Appendix C. Significantly, α_k is similar to the step size in other deep unfolding algorithms [37], [34], but it is a parameter to balance the noise and the reconstruction abilities of the module in this paper. Therefore, α_k is named as the balance parameter, and (11) would degenerates to (10) when α_k equals 1.

By extending (11) to the reconstruction of the whole image, the mathematical expression of the denoising module of the k -th reconstruction module is as follows:

$$\mathbf{X}^k = \mathfrak{S}^{-1}(\text{vec}^{-1}(\alpha_k \mathbf{A}^T \mathbf{Z}^{k-1} + \text{vec}(\mathfrak{S}(\mathbf{X}^{k-1}, n)) - \mathbf{H}^k \text{vec}(\mathfrak{N}_k(\mathfrak{S}(\mathbf{X}^{k-1}, n))), n), \quad (12)$$

where

$$\mathbf{H}^k = \alpha_k \mathbf{A}^T \mathbf{A} - \mathbf{I}, \quad (13)$$

$$\mathbf{Z}^{k-1} = \mathbf{Y} - \mathbf{A} \text{vec}(\mathfrak{S}(\mathbf{X}^{k-1}, n)). \quad (14)$$

Algorithm 1 The forward propagation of AMP-Net- K **Input:** $\bar{\mathbf{X}}, \mathbf{A}, \mathbf{B}, \alpha, \Theta, \Omega, n, K$ **Output:** output \mathbf{X}^K **Sampling process:**

$$\mathbf{Y} = \mathbf{A} \operatorname{vec}(\mathfrak{S}(\bar{\mathbf{X}}, n))$$

Reconstruction process:

- 1: Set $k = 0$
- 2: $\mathbf{X}^k = \mathfrak{S}^{-1}(\operatorname{vec}^{-1}(\mathbf{B}\mathbf{Y}))$
- 3: **for** $k < K$ **do**
- 4: $k = k + 1$
- 5: $\mathbf{H}^k = \alpha_k \mathbf{A}^T \mathbf{A} - \mathbf{I}$
- 6: $\mathbf{Z}^{k-1} = \mathbf{Y} - \mathbf{A} \operatorname{vec}(\mathfrak{S}(\mathbf{X}^{k-1}, n))$
- 7: $\mathbf{X}^k = \mathfrak{S}^{-1}(\operatorname{vec}^{-1}(\alpha_k \mathbf{A}^T \mathbf{A}^{k-1} + \operatorname{vec}(\mathfrak{S}(\mathbf{X}^{k-1}, n)) - \mathbf{H}^k \operatorname{vec}(\mathfrak{N}_k(\mathfrak{S}(\mathbf{X}^{k-1}, n))), n))$
- 8: $\mathbf{X}^k = \mathbf{X}^k - \mathfrak{B}_k(\mathbf{X}^k)$
- 9: **return** \mathbf{X}^k

TABLE I
THE COMPARISON BETWEEN AMP-NET AND OTHER STATE-OF-THE-ART METHODS.

Method	Trainability	Interpretation	Fixed computational complexity	Sampling matrix training	Deblocking operation	Regularization Term
TVAL3 [44]		✓				✓
D-AMP [14]		✓				✓
DCS [17]	✓	✓		✓		✓
ReconNet [27]	✓		✓			
CSNet ⁺ [28]	✓		✓	✓	✓	
ISTA-Net ⁺ [34]	✓	✓	✓			✓
DPDNN [36]	✓	✓	✓			✓
NN [41]	✓	✓	✓			✓
AMP-Net	✓	✓	✓	✓	✓	

And Fig. 4 provides a graphical illustration of the k -th reconstruction module of AMP-Net.

It is necessary to note that $\mathfrak{S}(\cdot, n)$, $\mathfrak{S}^{-1}(\cdot, n)$, $\operatorname{vec}(\cdot)$ and $\operatorname{vec}^{-1}(\cdot)$ do not introduce additional floating point calculations, but only for logically illustrating the process of image sampling and reconstruction, and further paving the way for the deblocking module.

Deblocking module. Reconstructing images block by block without overlapping may lead to a situation that additional deblocking operations must be carried out. To this end, a deblocking module is developed to eliminate the blocking artifact and further improve the reconstruction performance.

In detail, \mathbf{X}^k can be further expressed as $\mathbf{X}^k = \bar{\mathbf{X}} + \mathbf{E}$ where $\mathbf{E} \in \mathbb{R}^{L \times P}$ denotes the difference between the original image and the output of the k -th denoising module. To map \mathbf{X}^k to $\bar{\mathbf{X}}$, a non-linear learnable function $\mathfrak{B}_k(\cdot)$ is designed to fit \mathbf{E} . With similar structure of ResNet [48], the process of image deblocking in the k -th reconstruction module is illustrated in Fig. 4 and can be expressed as

$$\mathbf{X}_{\text{out}}^k = \mathbf{X}_{\text{in}}^k - \mathfrak{B}_k(\mathbf{X}_{\text{in}}^k), \quad (15)$$

where \mathbf{X}_{in}^k and $\mathbf{X}_{\text{out}}^k$ denote the input and the output, respectively. The input of $\mathfrak{B}_k(\cdot)$ is the whole concatenated image rather than each image block. In fact, $\mathfrak{B}_k(\cdot)$ is a CNN with the same structure as $\mathfrak{N}_k(\cdot)$ in this study but different parameter values. Significantly, this process can also be regarded as the further denoising of the image and processing the whole image gives AMP-Net the potential of image deblocking.

Theoretically, the denoising module and the deblocking module are important for the construction of the proposed model. Without denoising modules, AMP-Net degenerates to a classical deep network stacked by convolutional layers. And AMP-Net only samples and restores each image block individually if deblocking modules are removed, which would easily produce blocking artifacts.

C. Loss Function

The trainable parameters of AMP-Net contain the measurement matrix \mathbf{A} , initialization matrix \mathbf{B} , the balance parameters $\boldsymbol{\alpha} = \{\alpha_1, \alpha_2, \dots, \alpha_K\}$, all the trainable parameters in $\mathfrak{N}(\cdot)$ set as $\boldsymbol{\Theta} = \{\boldsymbol{\Theta}_1, \boldsymbol{\Theta}_2, \dots, \boldsymbol{\Theta}_K\}$, and all the trainable parameters in $\mathfrak{B}(\cdot)$ set as $\boldsymbol{\Omega} = \{\boldsymbol{\Omega}_1, \boldsymbol{\Omega}_2, \dots, \boldsymbol{\Omega}_K\}$. $\boldsymbol{\Theta}_k$ denotes the trainable parameters of $\mathfrak{N}_k(\cdot)$ and $\boldsymbol{\Omega}_k$ denotes the trainable parameters of $\mathfrak{B}_k(\cdot)$. Meanwhile, AMP-Net- K is named as the AMP-Net with K reconstruction modules. Algorithm 1 describes the forward propagation of AMP-Net- K which includes the sampling process and the reconstruction process.

In this paper, we use mean square error (MSE) to describe the difference between the original image and the recovered image. Then the loss function of AMP-Net- K can be formulated as

$$\mathcal{L}(\mathbf{A}, \mathbf{B}, \boldsymbol{\alpha}, \boldsymbol{\Theta}, \boldsymbol{\Omega}) = \frac{1}{N_a N_b} \sum_{m=1}^{N_b} \|\bar{\mathbf{X}}_m - \mathbf{X}_m^K\|_2^2, \quad (16)$$

where $\bar{\mathbf{X}}_m$ is the m -th original image in the training set, N_a denotes the size of $\bar{\mathbf{X}}_m$ and N_b denotes the size of the training set.

IV. EXPERIMENTAL RESULTS

In this section, experiments are performed on the visual image CS reconstruction. First, the proposed AMP-Net is compared with other state-of-the-art methods. And the performance of AMP-Net with different parameter sharing strategies is analyzed. Finally, we validated the effectiveness of deblocking modules and the sampling matrix training strategy.

A. Experimentally setting

All of our experiments are performed on two datasets: BSD500 [49] and Set11 [27]. BSD500 contains 500 colorful visual images which are divided into three parts: the training set (200 images), the validation set (100 images) and the test set (200 images). And Set11 [27] contains 11 grey-scale images. We use the luminance components of BSD500 for training, validation and testing, and use Set11 for testing.

In this study, we set the size n of each image block as 33. To train AMP-net, 448 sub images sized of 99×99 are randomly extracted from the luminance component of each image of the training set of BSD500. This training set contains 89600 images and each image is constructed with 9 image blocks. The validation set of BSD500 is used to choose the best model for testing. And the test set of BSD500 and Set11 are used for testing. Peak Signal-to-Noise Ratio (PSNR) and Structural Similarity Index (SSIM) are used for evaluation. The higher PSNR and SSIM are, the better the models performance. The average PSNR on validation set are calculated at the end of each training epoch, and the model with the highest PSNR is regarded as the best model for testing.

Before training, entries of \mathbf{A} are initialized randomly by Gaussian distribution and all the rows are orthogonalized. The balance parameter α_k of AMP-Net is initialized as 1, and other trainable parameters are initialized randomly. The optimization algorithm employed for training is Adam [45]. AMP-net are trained for 50 epochs with batch size 32 and learning rate 0.0001. In our experiments, we train three AMP-Nets with different number of reconstruction modules: AMP-Net-2, AMP-Net-4 and AMP-Net-6. Moreover, we train other trainable comparison methods by ourselves under the certain conditions mentioned in their related papers with the image block size as 33. All the experiments are implemented on a platform with an AMD Ryzen7 2700X CPU and a RTX2080Ti GPU.

B. Comparison with State-of-the-Art Methods

We compare AMP-Net-2, AMP-Net-4 and AMP-Net-6 with other eight state-of-the-art methods, namely TVAL3 [44], D-AMP [14], DCS [17], ReconNet [27], CSNet⁺ [28], ISTA-Net⁺ [34], DPDNN [36], NN [41]. TVAL3, D-AMP and DCS are model based methods. ReconNet and CSNet⁺ are classical deep network methods. And ISTA-Net⁺, DPDNN and NN are deep unfolding methods. Table I highlights the difference between these comparison methods and our method, in terms of whether to have interpretation, whether to have deblocking operations, whether to apply the sampling matrix training strategy and more.

Table II shows the test results on Set11 with different CS ratios of 50%, 40%, 30%, 25%, 10%, 4% and 1%. Table II contains the average PSNR (dB) and SSIM and the time-consuming analysis (average reconstruction time

TABLE II
THE TEST RESULTS OF EIGHT COMPARISON METHODS AND AMP-NET-2, AMP-NET-4 AND AMP-NET-6 ON SET11.

Method	50%	40%	30%	25%	10%	4%	1%	Time (s) CPU/GPU
	PSNR (dB)/SSIM							
TVAL3 [44]	33.39/0.8157	31.21/0.7531	29.00/0.6764	27.63/0.6238	22.45/0.3758	17.88/0.1997	14.90/0.0646	2.379/
D-AMP [14]	37.34/0.8504	35.22/0.8078	32.64/0.7544	31.62/0.7233	19.87/0.3757	11.28/0.0971	5.58/0.0034	39.139/
DCS [17]	22.30/0.5452	21.99/0.5033	21.98/0.5358	21.85/0.5116	21.53/0.4546	18.03/0.2202	17.12/0.3251	1.829/0.036
ReconNet [27]	32.34/0.9181	30.63/0.9019	29.16/0.8701	28.47/0.8533	24.46/0.7305	21.13/0.5903	17.58/0.4421	0.087/0.004
CSNet ⁺ [28]	38.19/0.9739	36.15/0.9625	33.90/0.9449	32.76/0.9322	27.76/0.8513	24.24/0.7412	20.09/0.5334	0.448/0.007
ISTA-Net ⁺ [34]	38.08/0.9680	35.93/0.9537	33.66/0.9330	32.27/0.9167	25.93/0.7840	21.14/0.5947	17.48/0.4403	1.126/0.027
DPDNN [36]	35.85/0.9532	34.30/0.9411	32.06/0.9145	30.63/0.8924	24.53/0.7392	21.11/0.6029	17.59/0.4459	2.439/0.058
NN [41]	31.41/0.8871	29.51/0.8523	27.64/0.8095	26.57/0.7842	22.99/0.6591	20.65/0.5525	17.67/0.4324	10.253/0.058
AMP-Net-2	39.48/0.9781	37.52/0.9686	35.21/0.9530	33.92/0.9417	28.67/0.8654	24.72/0.7562	20.41/0.5539	0.170/0.008
AMP-Net-4	40.07/0.9795	38.03/0.9705	35.67/0.9564	34.38/0.9451	29.05/0.8728	25.07/0.7680	20.35/0.5563	0.333/0.014
AMP-Net-6	40.27/0.9804	38.23/0.9713	35.90/0.9574	34.59/0.9477	29.45/0.8787	25.16/0.7692	20.57/0.5639	0.500/0.020

TABLE III
THE TEST RESULTS OF TWO NETWORK-BASED METHODS, THREE DEEP UNFOLDING METHODS, AMP-NET-2, AMP-NET-4 AND AMP-NET-6 ON THE TEST SET OF BSD500.

Method	50%	40%	30%	25%	10%	4%	1%	Parameter Number
	PSNR (dB)/SSIM							
ReconNet [27]	31.03/0.9001	29.60/0.8743	28.15/0.8335	27.46/0.8072	24.29/0.6755	21.84/0.5646	19.00/0.4530	22914
CSNet ⁺ [28]	35.89/0.9677	33.96/0.9513	31.94/0.9251	30.91/0.9067	27.01/0.7949	24.41/0.6747	21.42/0.5261	370560
ISTA-Net ⁺ [34]	34.92/0.9510	32.87/0.9264	30.77/0.8901	29.64/0.8638	25.11/0.7124	21.82/0.5661	18.92/0.4529	336978
DPDNN [36]	33.56/0.9373	32.05/0.9164	29.98/0.8759	28.87/0.8491	24.37/0.6863	21.80/0.5716	18.97/0.4544	1363712
NN [41]	30.47/0.8882	28.84/0.8511	27.23/0.8037	26.42/0.7757	23.44/0.6443	21.49/0.5451	19.06/0.4474	2954516
AMP-Net-2	36.89/0.9720	34.88/0.9567	32.74/0.9319	31.62/0.9134	27.50/0.8051	24.77/0.6873	21.77/0.5416	76418
AMP-Net-4	37.30/0.9735	35.22/0.9587	33.04/0.9348	31.88/0.9168	27.70/0.8108	24.92/0.6938	21.79/0.5473	152836
AMP-Net-6	37.48/0.9744	35.34/0.9594	33.17/0.9358	32.01/0.9188	27.82/0.8133	24.95/0.6949	21.90/0.5501	229254

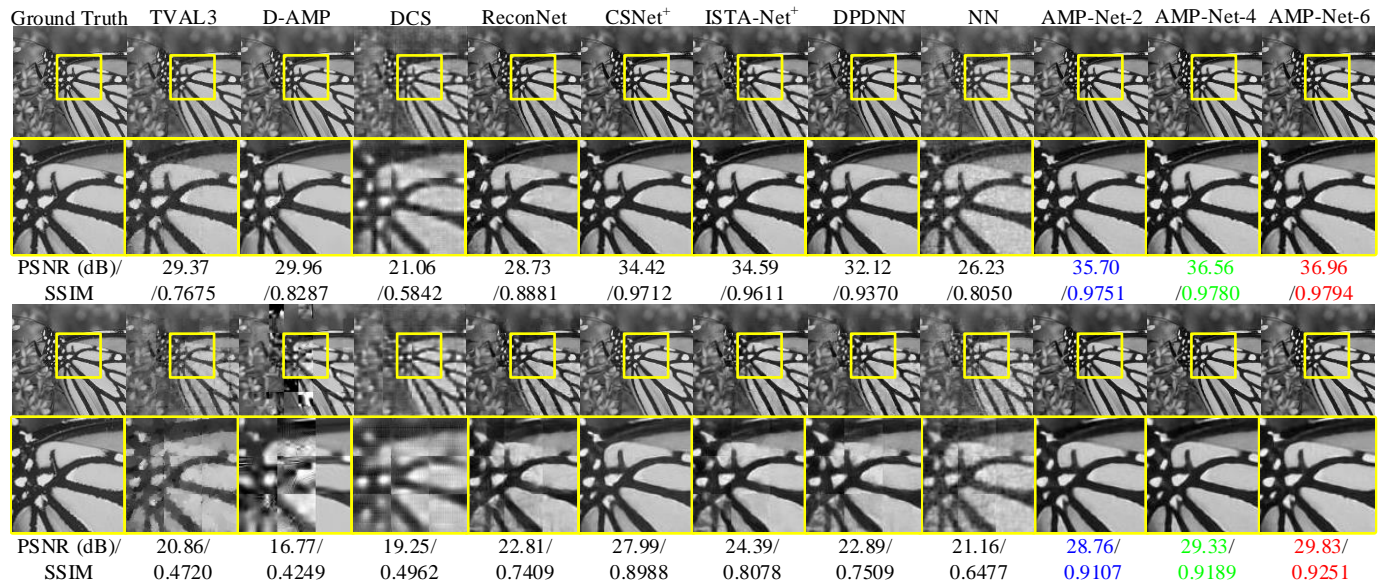


Fig. 5. The reconstruction results on *Monarch* image in Set11 with CS ratios of 30% and 10%. The first row is images reconstructed with CS ratio of 30% and the second row is images reconstructed with CS ratio of 10%.

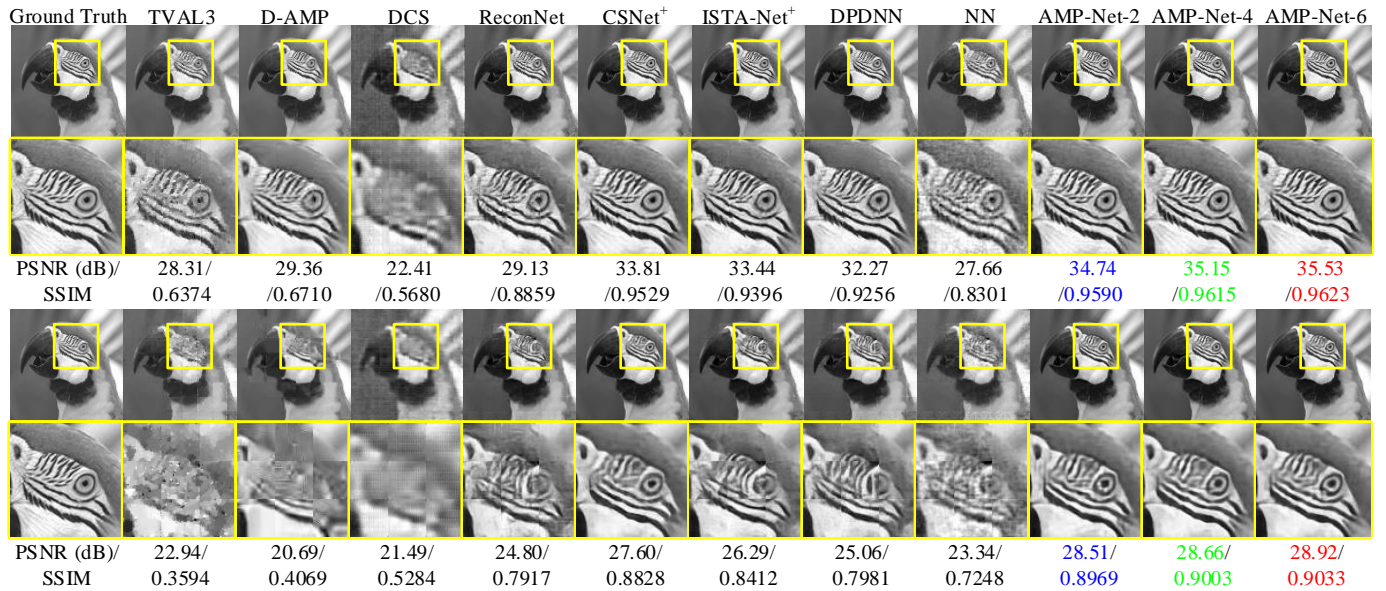


Fig. 6. The reconstruction results on *Parrots* image in Set11 with ratios of 30% and 10%. The first row is images reconstructed with CS ratio of 30% and the second row is images reconstructed with CS ratio of 10%.

of a 256×256 grayscale image) of each method, where the best, the second and the third results are marked with red font, green font and blue font, respectively.

From Table II, it can be found that TVAL3 and D-AMP have worse performance in low CS ratios of 4% and 1% than other methods. The performance of DCS has no distinct improvement when the CS ratio increases from 10% to 50%. Compared with TVAL3 and D-AMP, DCS does not have higher PSNR and SSIM with high CS ratios, but it performs better when the CS ratio is low. This is probably due to its only three-steps gradient descend process and the simple network structure. ReconNet does not work well in high CS ratios but in low CS ratios. And NN shows worse reconstruction results in high CS ratios of 50%, 40%, 30% and 25% but better results in 10%, 4%, 1% than three model based methods. As a deep unfolding method for common image inverse problem, DPDNN does not have a significant advantage in the image CS problem. However, ISTA-Net⁺ have a great improvement compared with TVAL3, D-AMP, DCS, ReconNet, DPDNN and NN in CS ratios of 50%, 40%, 30%, 25% and 10%. This shows that a well designed deep unfolding model have great potential in the image CS problem. As shown in Table II, CSNet⁺ beats the above seven methods with sampling matrix being trained. And AMP-Net outperforms all the eight methods with only two reconstruction modules. Meanwhile, as the number of reconstruction modules increases within a limited range, the results of AMP-Net get better.

From the last column of Table II, it costs a lot of time on image reconstruction for the three optimization-based methods using CPU or GPU. And ReconNet has the fastest reconstruction speed on CPU and GPU as a network-based method. The three AMP-Nets have lower computational consumption than the other three deep unfolding methods, while maintaining better reconstruction performance. It is worth noting that the CPU speed of AMP-Net-2 is only slower than ReconNet, and its GPU speed ranks third.

Fig. 5 and Fig. 6 show the reconstructed Monarch and Parrots images in Set11 with CS ratios of 30% and 10%. From Fig. 5 and 6, it can be seen that AMP-Net has much higher PSNR and SSIM than other methods. And as the number of reconstruction modules increases, PSNR and SSIM become higher. Meanwhile, there are no clearly visible blocking artifact in the AMP-Net reconstructed image. In addition, the reconstructed images with CS ratio of 30% contain more detailed information than with CS ratio of 10%. Therefore, in the experiments of next subsections, 30% and 10% are taken as the representative of the high CS ratio and the low CS ratio, respectively.

To further evaluate the generalization performance of AMP-Net, we compare AMP-Net-2, AMP-Net-4 and AMP-Net-6 with ReconNet, CSNet⁺, ISTA-Net⁺, DPDNN and NN on the test set of BSD500. Table III shows the average PSNR and SSIM and the parameter number of each model, where the best, the second and the third results are marked with red font, green font and blue font, respectively. It is necessary to note that the calculation of parameter numbers shown in Table III does not include **A** and **B**, because their parameter numbers vary with CS ratios. From Table III it is clear that AMP-Net has good generalization performance and has better performance than other

TABLE IV

THE TEST RESULTS OF AMP-NET-2, AMP-NET-4 AND AMP-NET-6 ON THE TEST SET OF BSD500 WITH DIFFERENT PARAMETER SHARING STRATEGIES.

CS Ratio	Module Number	Sharing Strategy	Parameter Number	PSNR (dB)/SSIM
30%	2	None	76418	32.74/0.9319
		α_k	76417	32.75/0.9320
		Θ_k, Ω_k	38210	32.68/0.9305
		$\alpha_k, \Theta_k, \Omega_k$	38209	32.67/0.9308
	4	None	152836	33.04/0.9348
		α_k	152833	33.06/0.9350
		Θ_k, Ω_k	38212	32.91/0.9330
		$\alpha_k, \Theta_k, \Omega_k$	38209	32.94/0.9332
	6	None	229254	33.17/0.9358
		α_k	229249	33.15/0.9361
		Θ_k, Ω_k	38214	33.03/0.9342
		$\alpha_k, \Theta_k, \Omega_k$	38209	33.05/0.9344
10%	2	None	76418	27.50/0.8051
		α_k	76417	27.48/0.8053
		Θ_k, Ω_k	38210	27.45/0.8039
		$\alpha_k, \Theta_k, \Omega_k$	38209	27.47/0.8038
	4	None	152836	27.70/0.8108
		α_k	152833	27.67/0.8100
		Θ_k, Ω_k	38212	27.60/0.8079
		$\alpha_k, \Theta_k, \Omega_k$	38209	27.63/0.8091
	6	None	229254	27.82/0.8133
		α_k	229249	27.77/0.8127
		Θ_k, Ω_k	38214	27.67/0.8090
		$\alpha_k, \Theta_k, \Omega_k$	38209	27.69/0.8100

five methods. And as the number of the reconstruction modules increases, the results of AMP-Net get better. In addition, the parameter numbers of the three AMP-Nets are smaller than three other three deep unfolding methods, and is only larger than ReconNet.

It is worth noting that without denoising modules, AMP-Net degenerates to a classical deep network with the similar structure as CSNet⁺. Table II and Table III show that AMP-Net has much higher PSNR and SSIM than CSNet⁺. Therefore, we claim that the deep unfolding structure of AMP-Net can highly improve the reconstruction performance.

C. Validating Different Parameter Sharing Strategies

In this subsection, we discuss the performance of AMP-Nets which employ different parameter sharing strategies.

Besides sampling matrix and initialization matrix, parameters of AMP-Net contain $\alpha = \{\alpha_1, \alpha_2, \dots, \alpha_K\}$, $\Theta = \{\Theta_1, \Theta_2, \dots, \Theta_K\}$, and $\Omega = \{\Omega_1, \Omega_2, \dots, \Omega_K\}$. For α_k , its parameter number is 1. And for Θ_k and Ω_k , their parameter numbers are both 19104 ($1 \times 32 \times 32 \times 3 \times 3 + 32 + (32 \times 32 \times 3 \times 3 + 32) \times 2 + 1 \times 32 \times 3 \times 3$). Table II contains the parameter number of all network-based methods and deep unfolding methods we compared, and AMP-Net-2, AMP-Net-4 and AMP-Net-6 with no parameter sharing strategy.

Table IV shows the average PSNR (dB) and SSIM of AMP-Net-2, AMP-Net-4 and AMP-Net-6 in different parameter sharing strategies tested on the test set of BSD500 with CS ratios of 30% and 10%. From Table IV, with the same number of reconstruction modules, AMP-Nets have similar reconstruction performance even with different parameter sharing strategies. Especially, with α_k , Θ_k and Ω_k being shared, AMP-Net can have a small parameter number which is only larger than ReconNet while maintaining good reconstruction results. From Table IV, it is clear that AMP-Net can be applied in devices with small storage space.

D. Validating the Capability of the Deblocking Module

In this subsection, we validate the deblocking ability of the deblocking module. Firstly, We name AMP-Net without deblocking modules as AMP-Net⁻. Then we train AMP-Net⁻ in the same condition as AMP-Net. Fig. 7 shows the reconstruction results of AMP-Net⁻ and AMP-Net with different number of reconstruction modules on Monarch and Parrots images in Set11 with CS ratio of 10%.

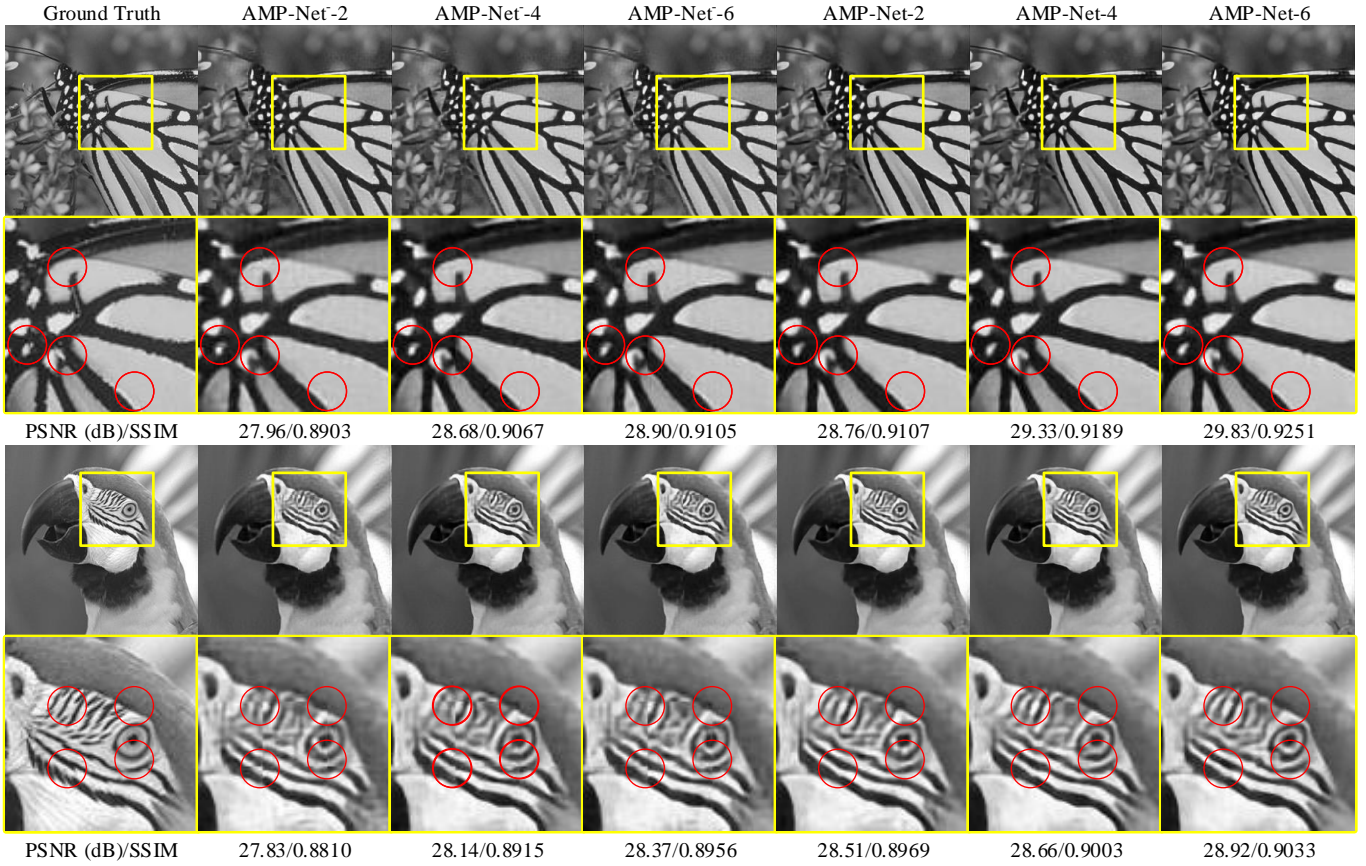


Fig. 7. The reconstruction results of AMP-Net⁺ and AMP-Net on *Monarch* and *Parrots* images in Set11 with CS ratio 10%.

Fig. 7 is quite revealing in several ways.

1) *The necessities of the deblocking module.* From Fig. 7, we can find that blocking artifact are clearly visible in the red-circle-marked areas of reconstructed images of AMP-Net⁺. And as the number of reconstruction modules decreases, the blocking artifact becomes more noticeable. Furthermore, there is no clearly visible blocking artifact in the image reconstructed by AMP-Net. In other words, it is necessary to include the deblocking modules into AMP-Net while achieving image reconstruction.

2) *The analysis of the deblocking ability.* Although AMP-Net and AMP-Net⁺ use the same training strategy, AMP-Net⁺ still generates images with blocking artifact. This means that blocking artifact will be inevitably introduced due to the block-by-block reconstruction of images. Therefore, it is difficult to achieve deblocking by simply using a training set composed of images, which are cascaded by image blocks. Moreover, the objects of the deblocking module are the whole images rather than each image block, which provides the potential for deblocking modules to deblock images generated by denoising modules.

3) *The performance improvement with the deblocking module.* Comparing the PSNR and SSIM value of each image in Fig. 7, AMP-Net have higher PSNR and SSIM than AMP-Net⁺. Therefore, we demonstrate that with deblocking modules, AMP-Net has better reconstruction performance than AMP-Net⁺.

E. Validating the Power of Sampling Matrix Training

In this subsection, we validate the improvement of reconstruction performance brought by the sampling matrix training strategy. Furthermore, we try to numerically prove that even without sampling matrix training strategy, AMP-Net can have better reconstruction performance than other deep unfolding methods.

We name AMP-Net without sampling matrix training strategy as AMP-Net^{*}. We compare AMP-Net^{*} with ISTA-Net⁺, DPDNN and NN with different number of reconstruction modules and different CS ratios. ISTA-Net⁺ in [34] has 9 reconstruction modules and is compared with AMP-Net^{*} with reconstruction module numbers of 2, 4, 6 and 9. As described in [36] and [41], the appropriate numbers of reconstruction modules of DPDNN and

TABLE V

THE TEST RESULTS OF ISTA-NET⁺, DPDNN, NN, AMP-NET* AND AMP-NET ON THE TEST SET OF BSD500 WITH DIFFERENT NUMBER OF RECONSTRUCTION MODULES.

Method	CS ratio 30%				CS ratio 10%			
	Reconstruction Module Number				Reconstruction Module Number			
	2	4	6	9	2	4	6	9
	PSNR (dB)/SSIM				PSNR (dB)/SSIM			
ISTA-Net ⁺ [34]	27.21/0.7962	29.61/0.8665	30.33/0.8818	30.77/0.8901	23.69/0.6483	24.59/0.6895	24.87/0.7021	25.11/0.7124
DPDNN [36]	28.04/0.8238	29.36/0.8617	29.98/0.8759		24.05/0.6725	24.32/0.6800	24.37/0.6863	
NN [41]	27.20/0.8021	27.21/0.8028	27.64/0.8029		23.46/0.6445	23.77/0.6537	23.74/0.6728	
AMP-Net*	30.12/0.8779	30.78/0.8912	31.04/0.8947	31.23/0.8974	25.09/0.7126	25.45/0.7265	25.67/0.7356	25.83/0.7488
AMP-Net	32.74/0.9319	33.04/0.9348	33.17/0.9358	33.24/0.9366	27.50/0.8051	27.70/0.8108	27.82/0.8133	27.84/0.8138

NN are chose to be 6, so we compare AMP-Net* with DPDNN and NN with the different reconstruction module numbers of 2, 4, and 6. Table V shows the average PSNR and SSIM of ISTA - Net⁺, DPDNN, NN, AMP-Net* and AMP-Net with different numbers of reconstruction modules tested on the test set of BSD500 with CS ratios of 30% and 10%, where the best is marked in bold and the second is underlined.

As can be seen from Table V, when the sampling rate and the number of reconstruction modules are the same, the PSNR and SSIM of AMP-Net are higher than AMP-Net*. Among them, PSNR is nearly 2dB higher, while SSIM is approximately 0.5dB higher. Therefore, we demonstrate that sampling matrix training strategy can improve the reconstruction performance of AMP-Net. Because the sampling matrix is used in the sampling and the reconstruction processes of AMP-Net, so obtaining a suitable sampling matrix might better help reconstruct the images.

From Table V, it can be observed that even without the sampling matrix training strategy, AMP-Net* can also obtain better reconstruction results than other deep unfolding methods. With the same number of reconstruction modules, AMP-Net* has higher PSNR and SSIM than ISTA-Net⁺, DPDNN and NN. Furthermore, with CS ratios of 30% and 10%, AMP-Net* with 2 reconstruction modules can obtain competitive performance or even better than ISTA-Net⁺ with 9 reconstruction modules, DPDNN and NN with 6 reconstruction modules.

F. Summary

In summary, based on the analysis above, the proposed AMP-Net is superior to other deep unfolding methods. There are several possible explanations for this result. Compared with ISTA-Net⁺, DPDNN and NN, AMP-Net builds a deep unfolding model with a different strategy from the denoising perspective of the AMP algorithm. Second, as shown in Section IV-D, the inclusion of deblocking modules can not only eliminate blocking artifact caused by block reconstruction, but also can improve the performance of AMP-Net. Third, the the sampling matrix training with other parameters simultaneously can help achieve better reconstruction. In general, a well designed framework brings AMP-Net an advantage in CS image reconstruction.

V. CONCLUSION

In this paper, we design a deep unfolding model named AMP-Net based on the denoising perspective of the AMP algorithm to solve the visual image CS problem. From experimental results, it is obvious that AMP-Net with only 2 reconstruction modules has better performance than other eight state-of-the-art methods. As the number of the reconstruction modules increases, the performance gets better. In addition, we find that with different parameter sharing strategies, AMP-Nets have similar performance with the same number of reconstruction modules, which means the parameter number of AMP-Net can be compressed efficiently. Finally, the effectiveness of the deblocking module and the sampling matrix training strategy is also verified.

APPENDIX A DERIVATION OF (4)

We have $\mathbf{y} = \mathbf{Ax}$ and $\mathbf{z}^k = \mathbf{y} - \mathbf{Ax}^k$. By combining two of them and the linear operation in (3), we can get

$$\mathbf{A}^T \mathbf{z}^0 + \mathbf{x}^0 = \mathbf{A}^T (\mathbf{y} - \mathbf{Ax}^0) + \mathbf{x}^0$$

$$\begin{aligned}
&= \mathbf{A}^T(\mathbf{A}\mathbf{x}^* - \mathbf{A}\mathbf{x}^0) + \mathbf{x}^0 \\
&= \mathbf{A}^T\mathbf{A}(\bar{\mathbf{x}} - \mathbf{x}^0) + \mathbf{x}^0 \\
&= \mathbf{A}^T\mathbf{A}(\bar{\mathbf{x}} - \mathbf{x}^0) - (\bar{\mathbf{x}} - \bar{\mathbf{x}}^0) + \bar{\mathbf{x}} \\
&= \bar{\mathbf{x}} + (\mathbf{A}^T\mathbf{A} - \mathbf{I})(\bar{\mathbf{x}} - \mathbf{x}^0)
\end{aligned} \tag{17}$$

In this way we can get (4).

APPENDIX B THE GRADIENT OF \mathbf{A}

Here we present the gradient of \mathbf{A} in the back propagation training process. Because the sampling matrix is used for processing image blocks in sampling and reconstruction, we only consider the one-block case. In addition, because $\mathfrak{S}(\cdot, n)$, $\mathfrak{S}^{-1}(\cdot, n)$, $\text{vec}(\cdot)$ and $\text{vec}^{-1}(\cdot)$ do not introduce floating point calculations, the gradients calculations can exclude them. Define the gradient of \mathbf{A} as $\nabla_{\mathbf{A}}\mathfrak{L} = \mathbf{A}_{\text{Sam}} + \mathbf{A}_{\text{Rec}}$, where \mathbf{A}_{Sam} is the gradient in the sampling model and \mathbf{A}_{Rec} denotes the gradient in the reconstruction model.

Assume that the gradient of \mathbf{x}_i^0 is known and is expressed as $\nabla_{\mathbf{x}_i^0}\mathfrak{L}$, then according to (7) and (8), \mathbf{A}_{Sam} can be written as

$$\mathbf{A}_{\text{Sam}} = \mathbf{B}^T \nabla_{\mathbf{x}_i^0} \mathfrak{L} \mathbf{x}_i^T. \tag{18}$$

\mathbf{A}_{Rec} can be expressed as

$$\mathbf{A}_{\text{Rec}} = \sum_{k=1}^K \mathbf{A}_{\text{Rec}}^k, \tag{19}$$

where $\mathbf{A}_{\text{Rec}}^k$ is the gradient in k -th reconstruction module and K is the the number of reconstruction modules. Assume that the gradient of \mathbf{x}_i^t is known and is expressed as $\nabla_{\mathbf{x}_i^t}\mathfrak{L}$, then according to (11), $\mathbf{A}_{\text{Rec}}^k$ can be expressed as

$$\mathbf{A}_{\text{Rec}}^k = \mathbf{A}_1^k + \mathbf{A}_2^k + \mathbf{A}_3^k, \tag{20}$$

where

$$\mathbf{A}_1^k = \alpha_k \nabla_{\mathbf{x}_i^k} \mathfrak{L} (\mathbf{y}_i - \mathbf{A}\mathbf{x}_i^{k-1})^T, \tag{21}$$

$$\mathbf{A}_2^k = \alpha_k \mathbf{S} \nabla_{\mathbf{x}_i^k} \mathfrak{L} (\bar{\mathbf{x}}_i - \mathbf{x}_i^{k-1})^T, \tag{22}$$

$$\mathbf{A}_3^k = -2\alpha_k \mathbf{S} \nabla_{\mathbf{x}_i^k} \mathfrak{L} \text{vec}(\mathfrak{N}_k(\mathbf{x}_i^{k-1})). \tag{23}$$

Furthermore, $\nabla_{\mathbf{x}_i^{k-1}}\mathfrak{L}$ can be calculated from $\nabla_{\mathbf{x}_i^k}\mathfrak{L}$. In detail, $\nabla_{\mathbf{x}_i^{k-1}}\mathfrak{L}$ can be expressed as

$$\begin{aligned}
\nabla_{\mathbf{x}_i^{k-1}}\mathfrak{L} &= -\alpha_k \mathbf{A}^T \mathbf{A} \nabla_{\mathbf{x}_i^k} \mathfrak{L} + \mathbf{1} \\
&\quad - [\nabla_{\mathbf{x}_i^{k-1}} \text{vec}(\mathfrak{N}_k(\mathbf{x}_i^{k-1}))]^T (\alpha_k \mathbf{A}^T \mathbf{A} - \mathbf{I}),
\end{aligned} \tag{24}$$

where $\mathbf{1} \in \mathbb{R}^{n^2}$ is a vctor of which each element equals 1.

APPENDIX C DERIVATION OF (11)

The same as (17), here we introduce a new parameter α , and we can get

$$\begin{aligned}
\alpha \mathbf{A}^T \mathbf{z}^0 + \mathbf{x}^0 &= \alpha \mathbf{A}^T (\mathbf{y} - \mathbf{A}\mathbf{x}^0) + \mathbf{x}^0 \\
&= \alpha \mathbf{A}^T (\mathbf{A}\bar{\mathbf{x}} - \mathbf{A}\mathbf{x}^0) + \mathbf{x}^0 \\
&= \alpha \mathbf{A}^T \mathbf{A} (\bar{\mathbf{x}} - \mathbf{x}^0) + \mathbf{x}^0 \\
&= \alpha \mathbf{A}^T \mathbf{A} (\bar{\mathbf{x}} - \mathbf{x}^0) - (\bar{\mathbf{x}} - \mathbf{x}^0) + \bar{\mathbf{x}} \\
&= \bar{\mathbf{x}} + (\alpha \mathbf{A}^T \mathbf{A} - \mathbf{I})(\bar{\mathbf{x}} - \mathbf{x}^0)
\end{aligned} \tag{25}$$

By applying (25) into the image block process and developing it to the iterative version, we can get

$$\begin{aligned}\mathbf{x}_i^k = & \alpha_k \mathbf{A}^T \mathbf{z}_i^{k-1} + \mathbf{x}_i^{k-1} \\ & - (\alpha_k \mathbf{A}^T \mathbf{A} - \mathbf{I}) \operatorname{vec}(\mathfrak{N}_k(\mathbf{X}_i^{k-1}))\end{aligned}\quad (26)$$

The process above is the derivation of (11).

REFERENCES

- [1] E. J. Candès and M. B. Wakin, "An introduction to compressive sampling [a sensing/sampling paradigm that goes against the common knowledge in data acquisition]," *IEEE Signal Processing Magazine*, vol. 25, no. 2, pp. 21–30, 2008.
- [2] M. F. Duarte, M. A. Davenport, D. Takhar, J. N. Laska, T. Sun, K. F. Kelly, and R. G. Baraniuk, "Single-pixel imaging via compressive sampling," *IEEE Signal Processing Magazine*, vol. 25, no. 2, pp. 83–91, 2008.
- [3] Y. Liu, S. Wu, X. Huang, B. Chen, and C. Zhu, "Hybrid CS-DMRI : Periodic time-variant subsampling and omnidirectional total variation based reconstruction," *IEEE Transactions on Medical Imaging*, vol. 36, no. 10, pp. 2148–2159, 2017.
- [4] J. Ma, X.-Y. Liu, Z. Shou, and X. Yuan, "Deep tensor ADMM-Net for snapshot compressive imaging," in *Proceedings of the IEEE International Conference on Computer Vision*, 2019, pp. 10223–10232.
- [5] R. G. Baraniuk, V. Cevher, M. F. Duarte, and C. Hegde, "Model-based compressive sensing," *IEEE Transactions on Information Theory*, vol. 56, no. 4, pp. 1982–2001, 2010.
- [6] S. Mallat, *A wavelet tour of signal processing*. Elsevier, 1999.
- [7] M. Elad, *Sparse and redundant representations: from theory to applications in signal and image processing*. Springer Science & Business Media, 2010.
- [8] S. Nam, M. Davies, M. Elad, and R. Gribonval, "The cosparse analysis model and algorithms?" *Applied and Computational Harmonic Analysis*, vol. 34, pp. 30–56, 2013.
- [9] J.-F. Cai, E. J. Candès, and Z. Shen, "A singular value thresholding algorithm for matrix completion," *SIAM Journal on Optimization*, vol. 20, no. 4, pp. 1956–1982, 2010.
- [10] Z. Long, Y. Liu, L. Chen, and C. Zhu, "Low rank tensor completion for multiway visual data," *Signal Processing*, vol. 155, pp. 301–316, 2019.
- [11] Y. Liu, Z. Long, and C. Zhu, "Image completion using low tensor tree rank and total variation minimization," *IEEE Transactions on Multimedia*, vol. 21, no. 2, pp. 338–350, 2019.
- [12] Y. Liu, Z. Long, H. Huang, and C. Zhu, "Low CP rank and Tucker rank tensor completion for estimating missing components in image data," *IEEE Transactions on Circuits and Systems for Video Technology*, 2019.
- [13] Y. Liu, M. De Vos, I. Gligorijevic, V. Matic, Y. Li, and S. Van Huffel, "Multi-structural signal recovery for biomedical compressive sensing," *IEEE Transactions on Biomedical Engineering*, vol. 60, no. 10, pp. 2794–2805, 2013.
- [14] C. A. Metzler, A. Maleki, and R. G. Baraniuk, "From denoising to compressed sensing," *IEEE Transactions on Information Theory*, vol. 62, no. 9, pp. 5117–5144, 2016.
- [15] K. Zhang, W. Zuo, S. Gu, and L. Zhang, "Learning deep CNN denoiser prior for image restoration," in *The IEEE Conference on Computer Vision and Pattern Recognition*, 2017, pp. 3929–3938.
- [16] D. Ulyanov, A. Vedaldi, and V. Lempitsky, "Deep image prior," in *The IEEE Conference on Computer Vision and Pattern Recognition*, 2018, pp. 9446–9454.
- [17] Y. Wu, M. Rosca, and T. Lillicrap, "Deep compressed sensing," in *The Thirty-sixth International Conference on Machine Learning (ICML 2019)*, 2019.
- [18] J. A. Tropp and S. J. Wright, "Computational methods for sparse solution of linear inverse problems," *Proceedings of the IEEE*, vol. 98, no. 6, pp. 948–958, 2010.
- [19] E. J. Candes and Y. Plan, "Matrix completion with noise," *Proceedings of the IEEE*, vol. 98, no. 6, pp. 925–936, 2010.
- [20] D. P. Wipf and B. D. Rao, "Sparse bayesian learning for basis selection," *IEEE Transactions on Signal Processing*, vol. 52, no. 8, pp. 2153–2164, 2004.
- [21] J. A. Tropp and A. C. Gilbert, "Signal recovery from random measurements via orthogonal matching pursuit," *IEEE Transactions on Information Theory*, vol. 53, no. 12, pp. 4655–4666, 2007.
- [22] A. Beck and M. Teboulle, "A fast iterative shrinkage-thresholding algorithm for linear inverse problems," *SIAM Journal on Imaging Sciences*, vol. 2, no. 1, pp. 183–202, 2009.
- [23] D. L. Donoho, A. Maleki, and A. Montanari, "Message-passing algorithms for compressed sensing," *Proceedings of the National Academy of Sciences*, vol. 106, no. 45, pp. 18914–18919, 2009.
- [24] S. Ravishankar, J. C. Ye, and J. A. Fessler, "Image reconstruction: From sparsity to data-adaptive methods and machine learning," *Proceedings of IEEE*, 2019.
- [25] C. Dong, C. C. Loy, K. He, and X. Tang, "Image super-resolution using deep convolutional networks," *IEEE Transactions on Pattern Analysis and Machine Intelligence*, vol. 38, no. 2, pp. 295–307, 2015.
- [26] A. Mousavi, A. B. Patel, and R. G. Baraniuk, "A deep learning approach to structured signal recovery," in *The 53rd Annual Allerton Conference on Communication, Control, and Computing*. IEEE, 2015, pp. 1336–1343.
- [27] K. Kulkarni, S. Lohit, P. Turaga, R. Kerviche, and A. Ashok, "Reconnet: Non-iterative reconstruction of images from compressively sensed measurements," in *The IEEE Conference on Computer Vision and Pattern Recognition*, 2016, pp. 449–458.
- [28] W. Shi, F. Jiang, S. Liu, and D. Zhao, "Image compressed sensing using convolutional neural network," *IEEE Transactions on Image Processing*, vol. 29, pp. 375–388, 2019.
- [29] W. Shi, F. Jiang, S. Liu, and D. Zhao, "Scalable convolutional neural network for image compressed sensing," in *The IEEE Conference on Computer Vision and Pattern Recognition*, 2019, pp. 12290–12299.

- [30] A. Krizhevsky, I. Sutskever, and G. E. Hinton, "Image-net classification with deep convolutional neural networks," in *Advances in Neural Information Processing Systems*, 2012, pp. 1097–1105.
- [31] I. Goodfellow, J. Pouget-Abadie, M. Mirza, B. Xu, D. Warde-Farley, S. Ozair, A. Courville, and Y. Bengio, "Generative adversarial nets," in *Advances in Neural Information Processing Systems*, 2014, pp. 2672–2680.
- [32] Y. Huang, T. Würfl, K. Breininger, L. Liu, G. Lauritsch, and A. Maier, "Some investigations on robustness of deep learning in limited angle tomography," in *International Conference on Medical Image Computing and Computer-Assisted Intervention*. Springer, 2018, pp. 145–153.
- [33] K. Gregor and Y. LeCun, "Learning fast approximations of sparse coding," in *The 27th International Conference on International Conference on Machine Learning*. Omnipress, 2010, pp. 399–406.
- [34] J. Zhang and B. Ghanem, "ISTA-Net : Interpretable optimization-inspired deep network for image compressive sensing," in *The IEEE Conference on Computer Vision and Pattern Recognition*, 2018, pp. 1828–1837.
- [35] J. Sun, H. Li, Z. Xu *et al.*, "Deep ADMM-Net for compressive sensing MRI , " in *Advances in Neural Information Processing Systems*, 2016, pp. 10–18.
- [36] W. Dong, P. Wang, W. Yin, G. Shi, F. Wu, and X. Lu, "Denoising prior driven deep neural network for image restoration," *IEEE Transactions on Pattern Analysis and Machine Intelligence*, vol. 41, no. 10, pp. 2305–2318, 2018.
- [37] X. Chen, J. Liu, Z. Wang, and W. Yin, "Theoretical linear convergence of unfolded ISTA and its practical weights and thresholds," in *Advances in Neural Information Processing Systems*, 2018, pp. 9061–9071.
- [38] M. Borgerding, P. Schniter, and S. Rangan, "AMP-inspired deep networks for sparse linear inverse problems," *IEEE Transactions on Signal Processing*, vol. 65, no. 16, pp. 4293–4308, 2017.
- [39] Z. Wang, Q. Ling, and T. S. Huang, "Learning deep l0 encoders," in *The Thirtieth AAAI Conference on Artificial Intelligence*, 2016.
- [40] J. Adler and O. Oktem, "Learned primal-dual reconstruction," *IEEE Transactions on Medical Imaging*, vol. 37, no. 6, pp. 1322–1332, 2018.
- [41] D. Gilton, G. Ongie, and R. Willett, "Neumann networks for linear inverse problems in imaging," *IEEE Transactions on Computational Imaging*, 2019.
- [42] S. G. Lingala, Y. Hu, E. DiBella, and M. Jacob, "Accelerated dynamic MRI exploiting sparsity and low-rank structure: kt SLR , " *IEEE Transactions on Medical Imaging*, vol. 30, no. 5, pp. 1042–1054, 2011.
- [43] S. Diamond, V. Sitzmann, F. Heide, and G. Wetzstein, "Unrolled optimization with deep priors," *arXiv preprint arXiv:1705.08041*, 2017.
- [44] C. Li, W. Yin, H. Jiang, and Y. Zhang, "An efficient augmented Lagrangian method with applications to total variation minimization," *Computational Optimization and Applications*, vol. 56, no. 3, pp. 507–530, 2013.
- [45] D. P. Kingma and J. Ba, " ADAM : A method for stochastic optimization," *International Conference on Learning Representations*, 2015.
- [46] S. Mun and J. E. Fowler, "Block compressed sensing of images using directional transforms," in *16th IEEE International Conference on Image Processing*. IEEE, 2009, pp. 3021–3024.
- [47] V. Nair and G. E. Hinton, "Rectified linear units improve restricted Boltzmann machines," in *The 27th International Conference on Machine Learning*, 2010, pp. 807–814.
- [48] K. He, X. Zhang, S. Ren, and J. Sun, "Deep residual learning for image recognition," in *The IEEE Conference on Computer Vision and Pattern Recognition*, 2016, pp. 770–778.
- [49] P. Arbelaez, M. Maire, C. Fowlkes, and J. Malik, "Contour detection and hierarchical image segmentation," *IEEE Transactions on Pattern Analysis and Machine Intelligence*, vol. 33, no. 5, pp. 898–916, 2010.